Poly(*N*-isopropylacrylamide) microgel swelling behavior and suspension structure studied with small-angle neutron scattering

B. Zhou[*] and U. Gasser[†,*]
Laboratory for Neutron Scattering and Imaging, Paul Scherrer Institut, 5232 Villigen, Switzerland

A. Fernandez-Nieves
Department of Condensed Matter Physics, University of Barcelona, 08028 Barcelona, Spain;
ICREA-Institucio Catalana de Recerca i Estudis Avancats, 08010 Barcelona, Spain;
and Institute for Complex Systems (UBICS), University of Barcelona, 08028 Barcelona, Spain

(Received 21 December 2022; revised 29 June 2023; accepted 11 September 2023; published 13 November 2023)

Microgels are of high interest for applications and as model systems due to their volume response to external stimuli. We use small-angle neutron scattering to measure the form and structure factors of poly(*N*-isopropylacrylamide) microgels in dilute and concentrated suspensions and find that microgels keep a constant size up to a concentration, above which they deswell. This happens before random-close packing. We emphasize suspension polydispersity must be considered to obtain accurate form and structure factors. Our results are compatible with microgel deswelling triggered by the osmotic pressure set by counterions associated to charged groups in the microgel periphery, which sharply increases when the counterion clouds surrounding the microgels percolate throughout the suspension volume.

DOI: 10.1103/PhysRevE.108.054604

I. INTRODUCTION

Microgels are cross-linked polymer particles suspended in a solvent that can change between swollen and deswollen states depending on external stimuli such as temperature [1,2], *p*H [3,4], and hydrostatic pressure [5–7]. This responsiveness is due to the softness of the polymer network. Temperature sensitive poly(*N*-isopropylacrylamide) (pNIPAM) microgels are among the most studied microgels due to their close-to-room-temperature lower critical solution temperature (LCST) $T_c \approx 32\,^{\circ}\mathrm{C}$ in H_2O. pNIPAM microgels are swollen by the solvent for $T < T_c$, and are deswollen at higher temperatures.

The effect of swelling on suspension behavior is highlighted by the spontaneous deswelling of large pNIPAM microgels surrounded by smaller but otherwise identical microgels above a critical concentration [8]. This selective deswelling reduces the polydispersity of the suspension, allowing for crystallization of suspensions that would otherwise not crystallize. In prior work, we showed that the osmotic pressure, π, due to counterions originating from charged groups located at the periphery of the pNIPAM microgels, Fig. 1(a), can lead to deswelling in concentrated suspensions, provided π is comparable or larger than the single-particle bulk modulus [9]. While most counterions are electrostatically bound to the microgel periphery, a fraction of them are bound with a strength comparable to the thermal energy kT, and are thus free to explore the suspension volume. These counterions determine the suspension osmotic pressure, as there are many more counterions than there are microgels. In contrast, at high particle concentrations, the counterion clouds surrounding all microgels begin to overlap, causing the bound counterions to progressively become free [9–11]; π is then controlled by these ions and becomes significantly larger relative to when there is no overlap between ion clouds, eventually causing microgel deswelling.

This model for deswelling in crowded suspensions suggests that the microgel size should stay constant with increasing particle concentration until the osmotic pressure is comparable to or exceeds the microgel bulk modulus. In contrast, an unexpected deswelling behavior of pNIPAM microgels at exceedingly low concentration was reported in prior work [2,12,13].

In this paper, we use small-angle neutron scattering (SANS) to study both the microgel form factor and the supension structure from dilute to overpacked conditions to follow changes in both the microgel size and internal structure, and the collective liquidlike structure factor of the suspension. Importantly, the polydispersity, which is ∼15%, is considered in both the form factor and the structure factor and is found to be essential to obtain reasonable results. In all studied suspensions, microgel deswelling starts at a volume fraction, ϕ, below random close packing, i.e., without direct contact between neighboring microgels.

II. MICROGEL SUSPENSIONS

We study four pNIPAM microgels with a crosslinker concentration of 2 mol% *N*, *N*′-methylene-bis-acrylamide (BIS) synthesized using precipitation polymerization at 70 °C, which is above the LCST of pNIPAM. Ammonium

[*]These authors contributed equally to this work.
[†]Corresponding author: urs.gasser@psi.ch

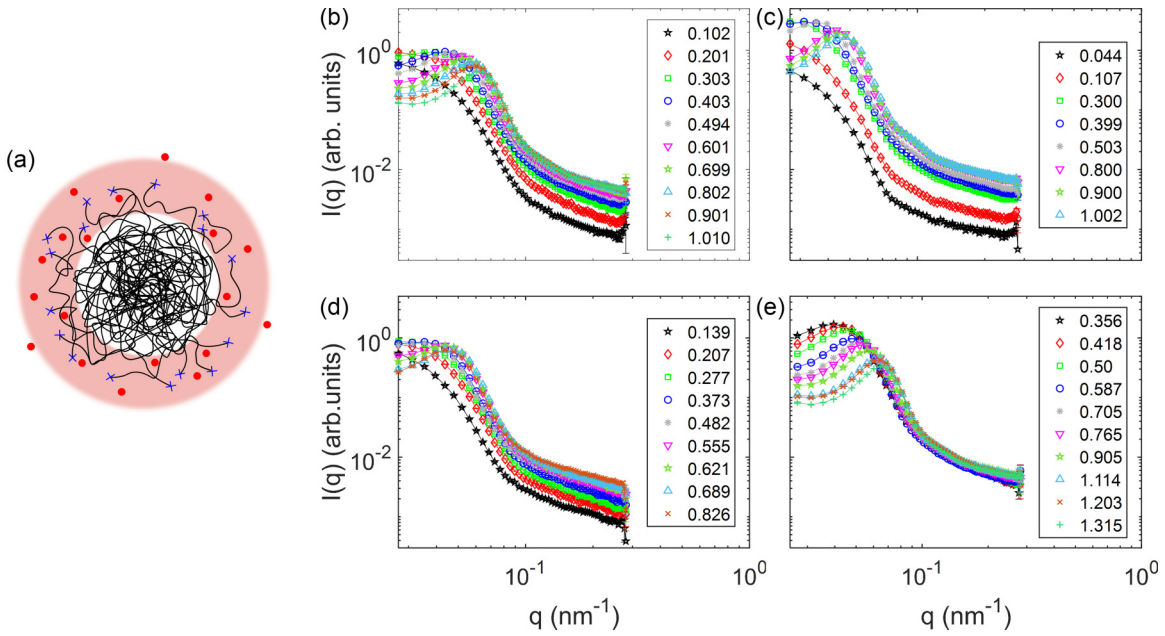

FIG. 1. (a) Sketch of a microgel with denser core and fuzzy corona. Charges at the ends of pNIPAM chains and counterions are represented by × and •, respectively. The red shaded area at the periphery represents the counterion cloud. (b)–(e) SANS curves for generalized volume fractions ζ given in the legends for samples s1 (b), s2 (c), s3 (d), and s4 (e).

persulfate [APS, $(NH_4)_2S_2O_8$] was used as the initiator of the polymerization reaction. To control the microgel size, we utilized the surfactant sodium dodecyl sulfate [SDS, $CH_3(CH_2)_{11}OSO_3Na$]. SDS stabilizes the primary particles, which are the seeds of the stable microgels, and grow by incorporating smaller precursor particles. By adding more SDS, smaller primary particles are obtained. Consequently, with a fixed amount of NIPAM monomer and BIS crosslinker, a larger number of smaller microgels is generated. The four pNIPAM microgels used in this study were synthesized following the same protocol and only the amount of SDS was varied, see Table I, to obtain microgels with different average radii and a polydispersity of ∼15%, which is relatively monodisperse for pNIPAM microgels [14]. During the synthesis, the BIS crosslinker reacts faster than NIPAM and, therefore, its concentration is higher in the initially formed core of the microgel, decaying in the fuzzy corona, which grows after most of the crosslinker has been used. This implies that larger microgels have a softer corona, as the crosslinker concentration would have decayed more from the core towards the periphery than for smaller microgels.

TABLE I. Hydrodynamic radius R_{sw} obtained with DLS at temperature T, the collapsed radius R_{coll}, the conversion constant k, and the amount of SDS used in synthesis for the four pNIPAM microgel samples.

Sample	T (°C)	R_{sw} (nm)	R_{coll} (nm)	k	SDS (mM)
s1	17.7	77.0 ± 0.6	25.5 ± 0.1	23.62 ± 0.03	3.00
s2	17.9	96.0 ± 0.8	34.51 ± 0.05	34.51 ± 0.05	2.00
s3	18.0	87.0 ± 1.0	28.17 ± 0.06	24.78 ± 0.04	2.50
s4	17.6	78.6 ± 0.6	27.65 ± 0.09	27.65 ± 0.09	2.95

Due to SDS and APS, Na^+ and NH_4^+ ions are present as mobile counterions, while -O-SO_2-O^- groups originating from APS remain at the end of the pNIPAM chains in the particle periphery. Information about the microgel synthesis can also be found in the Supplemental Material of Ref. [9]. After the synthesis, the microgel suspension is cleaned using dialysis to remove any unreacted monomers and SDS. The cleaned, final suspension of pNIPAM microgels thus contains Na^+ and NH_4^+ counterions. Most of these are electrostatically bound to the microgels. Using dynamic light scattering (DLS), we confirm the LCST of the particles is $T_c \approx 32\,^\circ$C in H_2O. We also find that the swollen radii at $T \approx 18\,^\circ$C is in the range from 77 nm to 96 nm for all four samples. To prepare microgel suspensions for SANS, the microgels are freeze dried and then resuspended in heavy water (D_2O). The change from H_2O to D_2O causes the LCST to increase from $T_c \approx 32\,^\circ$C to $\approx 33\,^\circ$C [15]. This slight change in the swelling behavior has no consequences for our study at $T \approx 18\,^\circ$C, far from the LCST.

Due to the softness and deformability of pNIPAM microgels, suspensions can be overpacked, forcing the particles to deform and deswell to fit in the available volume. This makes knowing the true volume fraction, ϕ, of the suspension difficult. Therefore, we use a generalized volume fraction

$$\zeta = \frac{N_{tot} V_{sw}}{V_{tot}} \approx \frac{m_p}{m_{tot}} \frac{\rho_s}{\rho_p} \frac{R_{sw}^3}{R_{coll}^3}, \tag{1}$$

where $V_{sw} = 4\pi R_{sw}^3/3$ is the fully swollen particle volume, and V_{tot}, m_{tot}, and m_p are the total volume and mass of the suspension, and the mass of the dry pNIPAM polymer, respectively. The density of the solvent ρ_s is that of D_2O, and $\rho_p = 1.269$ g/cm^3 [16] is the density of the pNIPAM polymer. The radii R_{sw} and R_{coll} correspond to the swollen and collapsed states, respectively; we measure R_{sw} using DLS (3D-DLS,

LS-Instruments, Fribourg, Switzerland) with a modified CONTIN algorithm [17], and obtain $R_{\rm coll}$ via viscosimetry (Ubbelohde viscosimeter, SI Analytics GmbH, Mainz, Germany), as explained below. Note $R_{\rm coll}$ is different from the deswollen radius reached at $T > T_{\rm c}$ where the microgels still contain a significant amount of solvent. For dilute suspensions, $\zeta = \phi$. Since microgels can deform, deswell, and interpenetrate, ζ can be larger than one, while the true volume fraction of spherical particles is limited to $\phi \leqslant \phi_{\rm rcp} \approx 0.64$ in disordered suspensions and to $\phi \leqslant \phi_{\rm cp} = \pi/(3\sqrt{2})$ in the crystalline state.

The collapsed radius $R_{\rm coll}$ in Eq. (1) is obtained from viscosimetry measurements taken at $T = (22.00 \pm 0.01)\,^{\circ}$C, yielding the relative viscosity $\eta_{\rm r} = \eta/\eta_{\rm H_2O}$ of five or six dilute suspensions with polymer mass fraction $c = m_{\rm p}/m_{\rm tot}$ in the range $10^{-4} \lesssim c \lesssim 4 \cdot 10^{-4}$. The collapsed radius is extracted from the $\eta_{\rm r}$ data using the Einstein-Batchelor relation [18–20]:

$$\begin{aligned}\eta_r &= 1 + 2.5\zeta + 5.9\zeta^2 \\ &= 1 + 2.5(kc) + 5.9(kc)^2,\end{aligned} \tag{2}$$

where we use $\zeta = kc$ and $k = \rho_{\rm s} R_{\rm sw}^3/(\rho_{\rm p} R_{\rm coll}^3)$, which depends on both $R_{\rm coll}$ and $R_{\rm sw}$. The viscosimetry measurements thus allow determining k and obtaining $R_{\rm coll}$ using $R_{\rm sw}$ obtained from DLS:

$$R_{\rm coll} = \left(\frac{\rho_{\rm s}}{\rho_{\rm p}}\frac{R_{\rm sw}^3}{k}\right)^{1/3}. \tag{3}$$

The radii $R_{\rm sw}$ and $R_{\rm coll}$, and the sample-dependent conversion constant k are summarized in Table I.

III. SMALL-ANGLE NEUTRON SCATTERING (SANS)

SANS measurements were taken on SANS-II at SINQ, Paul Scherrer Institut, with a wavelength of $\lambda = (1.08 \pm 0.04)$ nm and a sample-detector distance of $d_{\rm sd} = 6$ m at a temperature of $T \approx 18\,^{\circ}$C. The SANS data was corrected for dark counts and solvent (D_2O) background before calibration with an H_2O measurement following standard procedures [21]. The SANS curves obtained with concentration series of the four studied samples are shown in Figs. 1(b)–1(e). With increasing ζ, we notice the appearance of an interaction peak, which means that interparticle scattering becomes important. In addition, the peak position shifts to higher q as ζ increases, reflecting the decrease of the interparticle distance with increasing concentration. The scattering intensity, in arbitrary units, can be expressed as [22,23]

$$I(q) = n_{\rm d} V_p^2 \Delta\rho^2 P(q) S(q), \tag{4}$$

where $n_{\rm d} = N/V$ is the particle number density, and $\Delta\rho = \rho_{\rm p} - \rho_{\rm s}$ is the scattering contrast given by the difference of the scattering length densities (SLDs) of the pure polymer and the solvent. The factors $P(q)$ and $S(q)$ in Eq. (4) represent the particle form factor, with $P(q = 0) = 1$, and the suspension structure factor, respectively. This factorization is exact for monodisperse spherical particles in suspension but is an approximation when the suspension is polydisperse. In previous work, the polydispersity was considered only in the form factor, but its effect on the structure factor was completely neglected [12], in spite of the significant polydispersity of pNIPAM microgel suspensions, which is ∼15%. We use the so-called apparent structure factor [23,24], which is based on the assumption that the suspension structure is decoupled from polydispersity. We then replace the structure factor $S(q)$ of a monodisperse suspension with a corrected structure factor

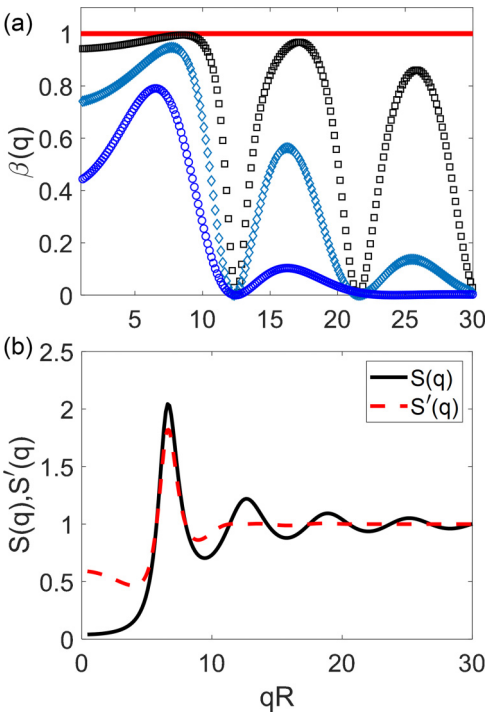

FIG. 2. (a) $\beta(q)$ calculated for polydispersities 0% (−), 8% (□), 18% (◇), and 30% (○). (b) Structure factors $S(q)$ (−) and $S'(q)$ (−−) calculated for particle radius 140 nm at $\zeta = 0.75$. $S(q)$ is for a monodisperse suspension and the apparent structure factor $S'(q)$ is calculated for a polydispersity of 30%.

$$S'(q) = 1 + \beta(q)(S(q) - 1), \tag{5}$$

$$\beta(q) = |\langle F_{\rm p}(q)\rangle|^2/\langle|F_{\rm p}(q)|^2\rangle, \tag{6}$$

where $\beta(q)$ is the so-called suppression factor, varying between zero and one, and $\langle\cdots\rangle$ represents an average with respect to the size distribution. While the numerator of $\beta(q)$ is based on the average scattering amplitude, conceptually standing for the form factor of a monodisperse suspension, the denominator contains a contribution due to the standard deviation $\delta F_{\rm p}(q)$ of the form factor, since $\delta F_{\rm p}^2(q) = \langle|F_{\rm p}(q)|^2\rangle - |\langle F_{\rm p}(q)\rangle|^2$. Thus, $\beta(q) = 1$ in the monodisperse case with vanishing $\delta F_{\rm p}(q)$, and $\beta(q) \to 0$ for highly polydisperse suspensions, where $\delta F_{\rm p}(q) \to \infty$. The q dependence of β for different polydispersities is shown in Fig. 2(a). The main effect of $\beta(q)$ is to suppress the characteristic oscillations of the liquidlike structure factor due to polydispersity; see Fig. 2(b). The monodisperse structure factor $S(q)$ of pNIPAM microgels up to rather high ζ is modeled using the Percus-Yevick result for hard spheres [25].

We use the fuzzy-sphere form factor, which is well accepted for microgels [10,12]. The single particle scattering

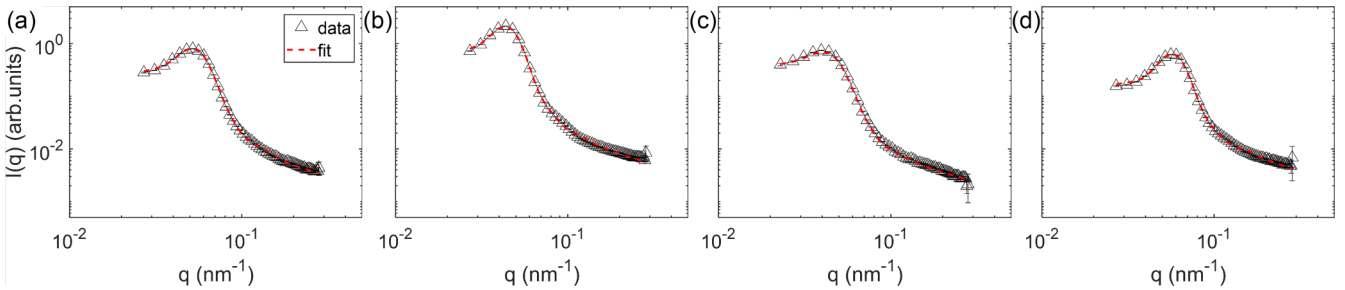

FIG. 3. SANS data (△) for samples s1 at $\zeta = 0.601$ (a), s2 at $\zeta = 0.80$ (b), s3 at $\zeta = 0.706$ (c), and s4 at $\zeta = 0.705$ (d) and fits to the data (−−) obtained using the model given in Eq. (10). For other SANS measurements, the model fits are as good as in the examples shown here or better.

amplitude in this model is

$$F_{\rm p}(q) = \frac{3[\sin(qR_{\rm c}) - qR_{\rm c}\cos(qR_{\rm c})]}{(qR_{\rm c})^3} \exp\left(-\frac{q^2\sigma_{\rm s}^2}{2}\right), \quad (7)$$

where R_c is the core radius of the microgel and $\sigma_{\rm s}$ is the half-width of its fuzzy shell. Eq. (7) is the Fourier transform of a sphere with radius $R_{\rm c}$ that is convolved with a Gaussian to obtain a corona with the density decreasing toward the particle periphery over the width $2\sigma_{\rm s}$ [2]. The radius of the particle is thus calculated as $R_{\rm SANS} = R_{\rm c} + 2\sigma_{\rm s}$. The form factor is defined as $P(q) = \langle|F(q)|^2\rangle/\langle|F(0)|^2\rangle$.

We introduce polydispersity in $P(q)$ using a log-normal distribution of the core radius with a standard deviation of σ:

$$D(R) = \frac{1}{R}\frac{1}{\sqrt{2\pi}\sigma}\exp\left(-\frac{(\ln R - \mu)^2}{2\sigma^2}\right), \quad (8)$$

where the average core radius is given by $\langle R\rangle = e^{\mu+\frac{\sigma}{2}}$, and the polydispersity is $\langle(R - \langle R\rangle)^2\rangle/\langle R\rangle^2 = e^{\sigma^2} - 1$. The form factor is then convoluted with $D(R)$ [Eq. (8)],

$$P_{\rm poly}(q) = \frac{1}{\langle V^2\rangle}\int_0^\infty D(R_{\rm c})V^2(R_{\rm c})P(q)dR_{\rm c}, \quad (9)$$

where $V(R_{\rm c}) = 4\pi R_{\rm c}^3/3$ is the volume of the core and $\langle V^2\rangle = \int_0^\infty D(R_{\rm c})V^2(R_{\rm c})dR_{\rm c}$ is the average-squared-core volume. As shown in a simulation study [26], the apparent structure factor is valid for moderate polydispersities and concentrations, and breaks down for significant polydispersities and high concentration, where the matrix form of the Ornstein-Zernicke equation for the pair potential needs to be solved to obtain a valid structure factor [27,28]. For the suspensions studied here, the polydispersity is ∼15% and the highest volume fraction is limited to $\phi < 0.5$ due to microgel deswelling. No crystalline phase is observed either. Therefore, we use the apparent structure factor as a good approximation to model the effect of polydispersity on $S(q)$. Including polydispersity, the scattering signal becomes

$$I_{\rm poly}(q) = n_{\rm d}\langle V^2\rangle\Delta\rho^2 P_{\rm poly}(q)S'(q).$$

Finally, we consider the instrument resolution by convoluting $I_{\rm poly}(q)$ with a Gaussian [29],

$$I(q) = \frac{1}{\sqrt{2\pi}\sigma_{\rm r}(q)}\int_0^\infty \exp\left(-\frac{(q-q')^2}{2\sigma_{\rm r}^2(q)}\right) I_{\rm poly}(q')\,dq' + I_{\rm chain}(q) + B, \quad (10)$$

where we have also included the scattering due to inhomogeneities within the polymer mesh of the microgel using a Lorentzian term, $I_{\rm chain}(q) = I_{\rm chain}(0)/[1 + (\xi q)^2]$, with ξ the correlation length given by the polymer-network-mesh size, and $I_{\rm chain}(0)$ the intensity of this contribution at $q = 0$ [30,31]. Additionally, the constant B represents the background due to incoherent scattering. All in all, Eq. (10) is the model that we use to describe our SANS data.

IV. RESULTS AND DISCUSSION

Using the model given by Eq. (10), we extract the parameters $R_{\rm c}$, $\sigma_{\rm s}$, σ, $I_{\rm chain}(0)$, and ξ defining the microgel form factor and the parameters $n_{\rm d}$ and $R_{\rm SANS} = R_{\rm c} + 2\sigma_{\rm s}$ relevant for the suspension structure given by $S'(q)$, see Table II. We start with the suspension with the lowest concentration at $\zeta \lesssim 0.1$, where the structure factor is essentially equal to one, and obtain the parameters for the form factor. The result is then used to start the analysis of the suspension with the next higher ζ, where we now include the structure factor. This scheme is repeated up to the highest concentration we probe in our experiments. In Fig. 3, we show the fit result at $\zeta \approx 0.75$ for each sample. Note that the structure factor depends on the microgel diameter and that $n_{\rm d}$ is calculated with the radius $R_{\rm SANS}$ obtained with the fuzzy-sphere model. Both the peak due to the structure factor and the intensity decay at higher q are very well captured by the model.

In addition to the Percus-Yevick structure factor, we have also applied the mean-spherical approximation (MSA) closure to use a structure factor that accounts for charges on the particles. The quality of the fits, however, did not at all improve. Furthermore, the effective charge of the microgels, used as a fitting parameter, was found to take on very low values, confirming the validity of the Percus-Yevick structure factor when applied to our system. This may be understood by considering that the open structure of the microgels appears to allow for an effective screening of the charged groups in the microgel periphery [11], together with the fact that microgel deswelling suppresses the influence of charges on the suspension structure due to the associated decrease in the suspension volume fraction ϕ.

The results obtained with the model given by Eq. (10) are summarized in Fig. 4. For samples s1, s2, and s3, the microgel volume is constant at the lowest measured concentrations, as shown by the low-ζ plateaus of $R_{\rm SANS}$ and $R_{\rm c}$. An osmotic pressure difference between the interior of the microgel and

TABLE II. Generalized volume fraction, ζ, core radius, R_c, half width of the fuzzy shell, σ_s, SANS radius, R_{SANS}, volume fraction, ϕ, polydispersity, PD, and the mesh size, ξ, for all studied suspensions of samples s1, s2, s3, and s4. R_c, σ_s, PD, and ξ are fit parameters, see Eqs. (7)–(10).

Sample	ζ ± 0.05	R_c (nm)	σ_s (nm)	R_{SANS} (nm)	ϕ	PD	ξ (nm)
s1	0.102	47.37 ± 0.47	12.05 ± 0.92	71.47 ± 2.3	0.04 ± 0.01	0.194 ± 0.015	9.50 ± 3.93
s1	0.201	46.31 ± 0.23	11.93 ± 0.23	70.18 ± 0.69	0.18 ± 0.003	0.199 ± 0.008	9.07 ± 0.92
s1	0.303	45.78 ± 0.17	12.10 ± 0.15	69.99 ± 0.46	0.29 ± 0.003	0.172 ± 0.010	13.24 ± 0.99
s1	0.403	45.15 ± 0.12	11.22 ± 0.08	67.58 ± 0.28	0.36 ± 0.001	0.151 ± 0.005	15.63 ± 0.84
s1	0.494	43.98 ± 0.06	10.62 ± 0.04	65.22 ± 0.14	0.39 ± 0.001	0.132 ± 0.025	15.03 ± 1.23
s1	0.601	42.11 ± 0.03	9.64 ± 0.02	61.39 ± 0.08	0.41 ± 0.001	0.114 ± 0.010	12.72 ± 0.48
s1	0.699	40.82 ± 0.03	9.26 ± 0.02	59.33 ± 0.07	0.42 ± 0.001	0.106 ± 0.010	12.68 ± 0.24
s1	0.802	39.49 ± 0.03	8.68 ± 0.02	56.86 ± 0.06	0.43 ± 0.001	0.102 ± 0.015	11.28 ± 0.79
s1	0.901	38.16 ± 0.03	8.28 ± 0.02	54.91 ± 0.06	0.43 ± 0.001	0.099 ± 0.010	8.49 ± 2.23
s1	1.01	36.79 ± 0.03	7.97 ± 0.02	52.73 ± 0.07	0.43 ± 0.001	0.098 ± 0.020	14.79 ± 0.42
s2	0.044	58.1 ± 0.46	17.5 ± 0.51	93.1 ± 1.49	0.02 ± 0.003	0.209 ± 0.004	10.68 ± 2.08
s2	0.107	58.0 ± 0.27	17.2 ± 0.49	92.4 ± 1.26	0.08 ± 0.003	0.214 ± 0.008	17.95 ± 6.36
s2	0.30	58.82 ± 0.04	17.08 ± 0.04	92.98 ± 0.13	0.26 ± 0.003	0.169 ± 0.008	15.09 ± 1.35
s2	0.399	58.82 ± 0.03	15.69 ± 0.02	90.20 ± 0.07	0.35 ± 0.001	0.157 ± 0.007	14.99 ± 0.29
s2	0.503	57.98 ± 0.03	14.26 ± 0.02	86.50 ± 0.08	0.41 ± 0.001	0.162 ± 0.012	11.45 ± 0.18
s2	0.80	50.10 ± 0.01	14.22 ± 0.02	78.62 ± 0.02	0.50 ± 0.001	0.144 ± 0.015	14.98 ± 1.55
s2	0.90	49.78 ± 0.01	12.53 ± 0.01	74.85 ± 0.02	0.49 ± 0.001	0.126 ± 0.010	14.88 ± 1.67
s2	1.002	47.55 ± 0.01	12.53 ± 0.01	72.62 ± 0.02	0.49 ± 0.001	0.121 ± 0.013	15.05 ± 1.46
s3	0.119	53.00 ± 0.36	15.51 ± 0.33	84.00 ± 1.01	0.09 ± 0.01	0.210 ± 0.008	7.47 ± 0.52
s3	0.177	53.01 ± 0.58	15.37 ± 0.67	83.74 ± 1.92	0.13 ± 0.001	0.201 ± 0.007	9.97 ± 1.47
s3	0.237	52.90 ± 0.59	15.03 ± 0.54	82.96 ± 1.67	0.21 ± 0.008	0.198 ± 0.008	9.99 ± 1.09
s3	0.319	52.27 ± 0.48	14.14 ± 0.41	80.55 ± 1.28	0.27 ± 0.001	0.181 ± 0.010	9.01 ± 0.75
s3	0.412	52.86 ± 0.13	11.64 ± 0.10	76.13 ± 0.33	0.31 ± 0.001	0.188 ± 0.010	5.93 ± 0.19
s3	0.475	51.09 ± 0.19	12.18 ± 0.16	75.45 ± 0.51	0.36 ± 0.002	0.162 ± 0.020	7.81 ± 0.39
s3	0.531	50.12 ± 0.18	12.28 ± 0.15	74.69 ± 0.47	0.37 ± 0.001	0.149 ± 0.012	9.86 ± 0.44
s3	0.589	49.62 ± 0.11	11.27 ± 0.08	72.16 ± 0.26	0.38 ± 0.001	0.130 ± 0.015	9.98 ± 1.27
s3	0.706	47.79 ± 0.04	11.05 ± 0.03	69.89 ± 0.09	0.40 ± 0.001	0.124 ± 0.020	10.02 ± 0.84
s4	0.356	46.08 ± 0.07	12.79 ± 0.05	71.66 ± 0.17	0.33 ± 0.60	0.149 ± 0.004	10.07 ± 1.55
s4	0.418	45.72 ± 0.04	12.23 ± 0.03	70.17 ± 0.10	0.36 ± 0.37	0.131 ± 0.005	10.01 ± 1.22
s4	0.50	44.87 ± 0.03	11.48 ± 0.02	67.82 ± 0.07	0.39 ± 0.25	0.117 ± 0.008	9.99 ± 1.10
s4	0.587	43.37 ± 0.04	11.39 ± 0.03	66.16 ± 0.09	0.43 ± 0.55	0.124 ± 0.010	10.05 ± 0.88
s4	0.705	41.60 ± 0.03	10.66 ± 0.02	62.91 ± 0.08	0.44 ± 0.39	0.109 ± 0.010	12.65 ± 0.58
s4	0.765	40.08 ± 0.03	10.57 ± 0.02	61.23 ± 0.08	0.45 ± 0.29	0.108 ± 0.015	10.95 ± 1.02
s4	0.905	38.33 ± 0.03	9.81 ± 0.02	57.95 ± 0.07	0.45 ± 0.25	0.104 ± 0.010	10.02 ± 0.44
s4	1.114	36.66 ± 0.04	8.13 ± 0.02	52.92 ± 0.08	0.44 ± 0.18	0.094 ± 0.015	9.98 ± 1.89
s4	1.203	35.93 ± 0.03	8.14 ± 0.02	52.21 ± 0.08	0.44 ± 0.17	0.093 ± 0.010	10.66 ± 0.93
s4	1.315	35.34 ± 0.05	7.79 ± 0.03	50.92 ± 0.10	0.44 ± 0.19	0.092 ± 0.015	10.08 ± 0.73

its surrounding comparable to or exceeding the microgel bulk modulus has to be reached for the microgels to deswell. As we will show below, deswelling occurs at volume fractions below $\phi_{rcp} \approx 0.64$. This observation supports the deswelling due to an osmotic pressure increase possibly triggered by the percolation of counterion clouds surrounding the microgels [9,32], which naturally explains deswelling without direct contact. The fuzzy corona with width $2\sigma_s$ starts to deswell first, reflecting that it is softer than the denser and more crosslinked core of the microgel. At a slightly higher ζ, R_c also deswells, but the core is compressed to a lesser extent than the fuzzy corona, as shown by the rescaled $2\sigma_s$ data ($\otimes$ symbols) in Fig. 4.

While R_{SANS} and R_c are constant at $\zeta \lesssim 0.3$ for samples s1, s2, and s3, the shell and the core of the microgels in sample s4 decrease in the whole ζ range studied, which starts at $\zeta \approx 0.36$, significantly higher than the lowest ζ studied for samples s1, s2, and s3; see Fig. 4(d).

To obtain an estimate of the true volume fraction ϕ, we replace the fully swollen microgel radius R_{sw} used in Eq. (1) with the radius measured at ζ: $\phi = \zeta\,[R_{SANS}(\zeta)/R_{sw}]^3$. The result is shown in Figs. 5(a)–5(d). We find $\phi < \phi_{rcp}$ in all studied suspensions. For $\zeta \lesssim 0.3$, $\phi \approx \zeta$ reflecting that no deswelling takes place at these low and moderate concentrations. At higher ζ, $\phi < \zeta$, and eventually ϕ plateaus. This shows that the microgels must deswell with increasing ζ. To characterize the deswelling, we determine the nearest-neighbor distance from the observed peak positions q^* in $S(q)$: $d_{nn} = 2\pi/q^*$. With increasing ζ, d_{nn} decreases, as the microgels move closer to each other to fit into the available space. We fit the high-ζ data with the model $d_{nn} = c\,\zeta^{-k}$,

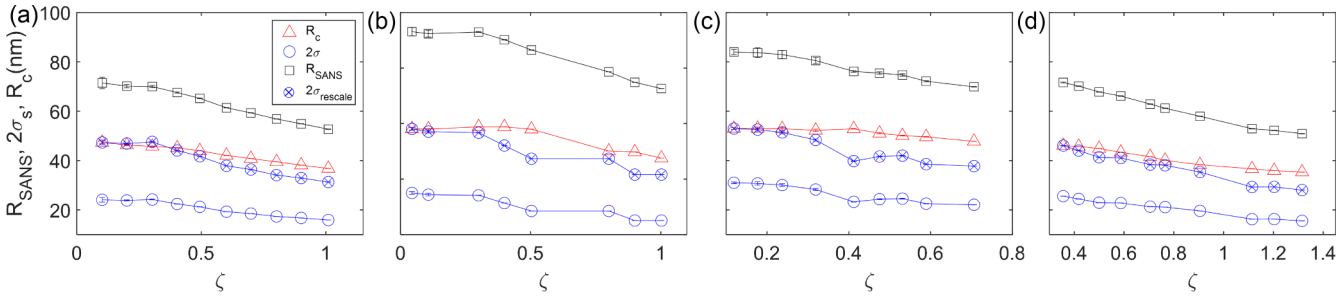

FIG. 4. R_{SANS} (□), R_c (△), and $2\sigma_s$ (○) of sample s1 (a), s2 (b), s3 (c), and s4 (d) versus generalized volume fraction ζ. $2\sigma_s$ rescaled for comparison with R_c is shown by ⊗. Lines are guides to the eye.

where c and k are fit parameters. As shown by the red curves in Figs. 5(e)–5(h), good agreement with the measured data is obtained for $k = 1/3$, which is expected for isotropic deswelling. Therefore, we find that microgels isotropically deswell without being in direct contact. Note that this scenario is supported by the fits to the measured SANS data using the model for spherical microgels given by Eq. (4). The fuzzy sphere model is found to apply up to the highest studied concentration, $\zeta \approx 1.3$, without signs for particle deformation or interpenetration; these could nevertheless occur at even higher ζ.

These results support our model for deswelling triggered by the percolation of counterion clouds in the space between microgels, which effectively frees previously bound counterions, allowing them to exert an osmotic pressure, π. The pressure in the interior of the microgels does not appreciably change, as the percolation of the clouds only alters the pressure outside the microgels. Therefore, a pressure difference between the inside and the outside, $\Delta\pi$, builds up, and microgel deswelling occurs when $\Delta\pi$ becomes comparable to or exceeds the microgel bulk modulus [9,11]. This scenario is expected to apply when the counterion clouds fill the space between the microgels.

To test whether our data support this scenario, we think of an effective particle consisting of a microgel and the surrounding cloud of counterions that are bound to the particle in dilute conditions [9,32]. In analogy to ζ, the effective volume fraction of these effective particles is $\zeta_{eff} = \zeta(\frac{R_{sw}+\Delta r}{R_{sw}})^3$, where Δr is the thickness of the counterion cloud located in the

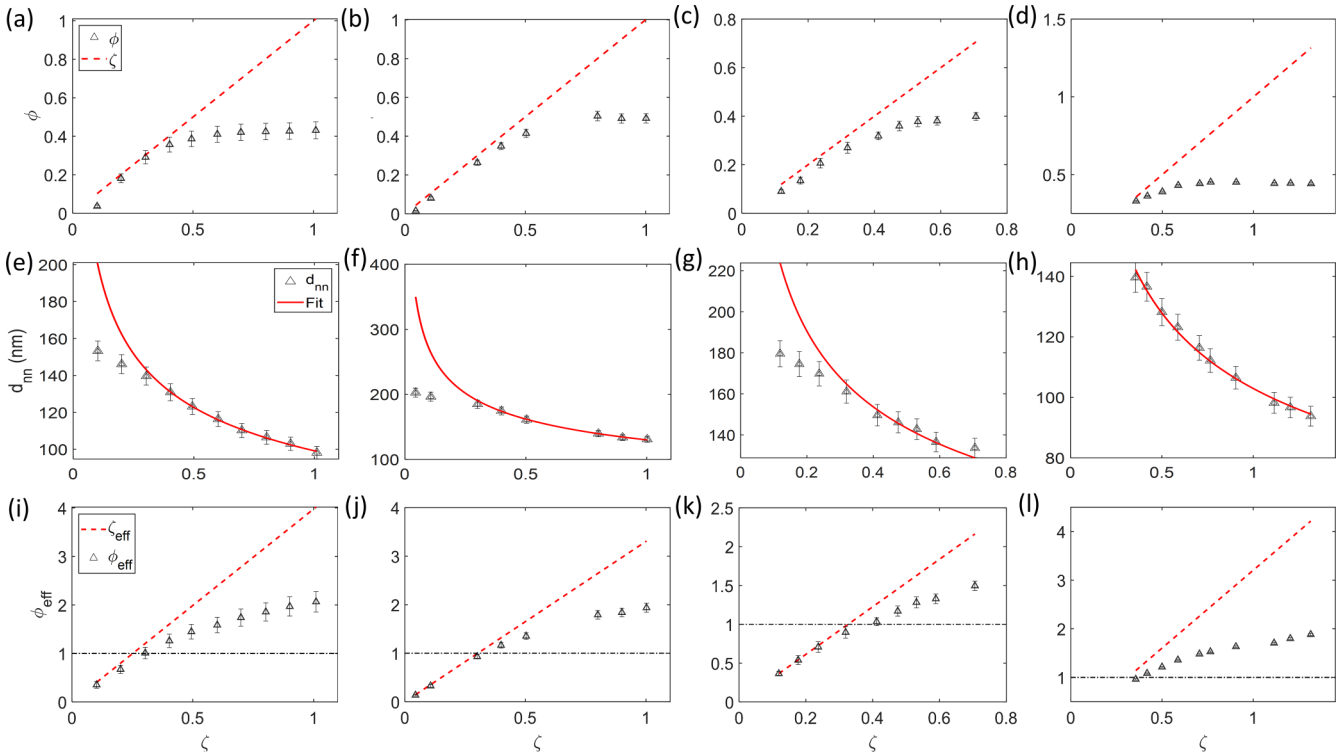

FIG. 5. (a)–(d): True volume fraction (△) of sample s1 (a), s2 (b), s3 (c), and s4 (d) versus generalized volume fraction ζ. The dashed lines represent $\phi = \zeta$. (e)–(h): Nearest-neighbor distances (△) in suspensions of sample s1 (e), s2 (f), s3 (g), and s4 (h). The red curves show fits to the high-q data with $d_{nn} = c\,\zeta^{-k}$. The fits are $99\,\zeta^{-0.32}$ (s1), $131\,\zeta^{-0.32}$ (s2), $122\,\zeta^{-0.31}$ (s3), and $103\,\zeta^{-0.33}$ (s4). (i)–(l): Calculated effective volume fraction $\phi_{eff}(\zeta)$ (△) for s1 (i), s2 (j), s3 (k), and s4 (l). The dashed line represents $\zeta_{eff}(\zeta)$. The dash dotted line highlights a volume fraction of one.

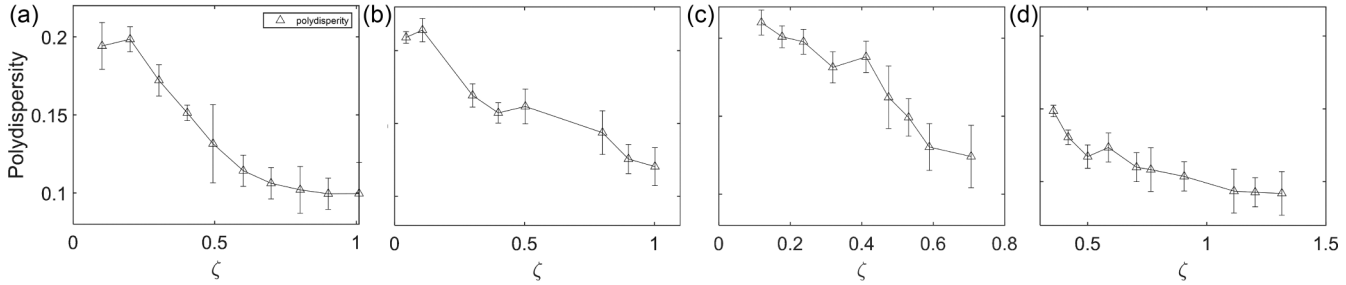

FIG. 6. Polydispersity (△) of samples s1 (a), s2 (b), s3 (c), and s4 (d) as a function of generalized volume fraction ζ. Lines are guides to the eye.

outside region of the microgel, see Fig. 1(a). In prior work, we obtained an estimate of $\Delta r = 35$ nm from measurements of the freezing point of polydisperse microgel suspensions [9,10]. Here, we estimate Δr using the condition that $\zeta_{\text{eff}}(\zeta) = 1$ [Figs. 5(i)–5(l)] when $R_{\text{SANS}}(\zeta)$ starts to decrease from the fully swollen size and, therefore, ϕ starts to deviate from ζ [Figs. 5(a)–5(d)]. We obtain $\Delta r = (44 \pm 5)$ nm (s1), (47 ± 5) nm (s2), (38 ± 6) nm (s3), and (37 ± 3) nm (s4), which are all in good agreement with the previously determined value. This condition is also reflected by comparing ζ_{eff} with the true volume fraction of the effective particles, defined by $\phi_{\text{eff}} = \zeta(\frac{R_{\text{SANS}}(\zeta)+\Delta r}{R_{\text{sw}}})^3$, shown by the triangles (△) in Figs. 5(i)–5(l). We find that ϕ_{eff} stays close to ζ_{eff} at the lowest concentrations, where the microgels retain their fully swollen state. As soon as deswelling begins, the curve given by ϕ_{eff} flattens in analogy to $\phi(\zeta)$; see Figs. 5(i)–5(l). For samples s1, s2, and s3, $\zeta_{\text{eff}} = 1$ is reached at $\zeta \approx 0.25$, 0.30, and 0.31, respectively.

With these observations, we can explain the apparently different behavior of sample s4. The lowest $\zeta \approx 0.36$ studied for this sample corresponds to $\zeta_{\text{eff}} \approx 1$, indicating the condition for percolation of the counterion clouds and for deswelling to occur has already been met. The microgels thus deswell in the whole studied ζ range and, as for the other samples, isotropic deswelling is observed, see Fig. 5(h). All these results support our model for microgel deswelling as a consequence of the percolation of counterion clouds.

As the largest microgels synthesized using precipitation polymerization are expected to be the softest, it is expected that the largest microgels deswell first and that suspension polydispersity decreases as $\zeta_{\text{eff}} > 1$. The polydispersities obtained from our SANS data indeed confirm this scenario, as shown in Fig. 6. In the fully swollen state, polydispersities are in the range from 0.15 to 0.22, and they are seen to decrease to values close to 0.1 at the highest studied ζ for all samples.

V. CONCLUSIONS

The presented SANS data for pNIPAM microgels with 2 mol% BIS crosslinker confirm our previous results for spontaneous microgel deswelling at high ζ triggered by the osmotic pressure increase due to the percolation of the counterion clouds surrounding the microgels. We find that microgels stay fully swollen up to $\zeta \approx 0.3$, and that it is at approximately this ζ that the percolation of counterion clouds first occurs. The observed critical concentration for deswelling agrees with the width of the counterion clouds determined in previous work [9–11]. Furthermore, the observed suspension polydispersity σ also supports the model for spontaneous deswelling. It decreases when deswelling occurs, as expected for suspensions with all microgels synthesized according to the same protocol [10]. We find the inclusion of polydispersity is essential to obtain consistent results for the microgel size and the suspension structure, particularly at low ζ, where deswelling should not have occurred. The apparent structure factor [Eq. (5)] appears to be sufficient for polydispersities $\lesssim$0.2. The suspension structure can be modeled with the Percus-Yevick structure factor for hard spheres, although the microgels carry charged groups and counterions at their periphery. The spontaneous deswelling at high concentrations and the resulting reduction in the volume fraction ϕ is likely an important factor to explain the apparently charge-neutral structure, as deswelling allows for more screening volume between the microgels, reducing the effect of charges. Additionally, microgels are open particles and the charges on the polymer network are partly screened within the particle. These considerations as well as polymer-solvent mixing, and polymer network elasticity must all be at the heart of improved models aimed at predicting the phase behavior [10,33–36] and the interaction [37] of these soft colloids at low and high concentrations.

ACKNOWLEDGMENTS

We thank the Swiss National Science Foundation (Grant No. 200020_184839), MCIN/AEI/10.13039/501100011033/FEDER, UE (Grant No. PID2021-122369NB-I00), and 2021 SGR-00450 for financial support. All SANS data was taken on the instrument SANS-II at SINQ, Paul Scherrer Institut, Switzerland.

[1] R. Pelton, Adv. Colloid Interface Sci. **85**, 1 (2000).
[2] M. Stieger, W. Richtering, J. Pedersen, and P. Lindner, J. Chem. Phys. **120**, 6197 (2004).
[3] T. Hoare and R. Pelton, Macromolecules **37**, 2544 (2004).
[4] P. S. Mohanty and W. Richtering, J. Phys. Chem. B **112**, 14692 (2008).

[5] J. J. Lietor-Santos, B. Sierra-Martin, R. Vavrin, Z. Hu, U. Gasser, and A. Fernandez-Nieves, Macromolecules **42**, 6225 (2009).
[6] J. J. Lietor-Santos, U. Gasser, R. Vavrin, Z. Hu, and A. Fernandez-Nieves, J. Chem. Phys. **133**, 034901 (2010).
[7] J. J. Lietor-Santos, B. Sierra-Martin, U. Gasser, and A. Fernandez-Nieves, Soft Matter **7**, 6370 (2011).
[8] A. S. J. Iyer and L. A. Lyon, Angew. Chem. Int. Ed. **48**, 4562 (2009).
[9] A. Scotti, U. Gasser, E. S. Herman, M. Pelaez-Fernandez, L. A. Lyon, and A. Fernandez-Nieves, Proc. Natl. Acad. Sci. USA **113**, 5576 (2016).
[10] A. Scotti, U. Gasser, E. S. Herman, J. Han, A. Menzel, L. A. Lyon, and A. Fernandez-Nieves, Phys. Rev. E **96**, 032609 (2017).
[11] U. Gasser, A. Scotti, and A. Fernandez-Nieves, Phys. Rev. E **99**, 042602 (2019).
[12] M. Stieger, J. Pedersen, P. Lindner, and W. Richtering, Langmuir **20**, 7283 (2004).
[13] P. S. Mohanty, D. Paloli, J. J. Crassous, E. Zaccarelli, and P. Schurtenberger, J. Chem. Phys. **140**, 094901 (2014).
[14] R. Pelton and T. Hoare, in *Microgel Suspensions: Fundamentals and Applications*, edited by A. Fernandez-Nieves, H. M. Wyss, J. Mattsson, and D. A. Weitz (WILEY-VCH Verlag GmbH & CO. KGaA, 2011), Chap. 1, pp. 3–32.
[15] P. Kujawa and F. M. Winnik, Macromolecules **34**, 4130 (2001).
[16] L. Zhang, E. S. Daniels, V. L. Dimonie, and A. Klein, J. Appl. Polym. Sci. **118**, 2502 (2010).
[17] A. Scotti, W. Liu, J. S. Hyatt, E. S. Herman, H. S. Choi, J. W. Kim, L. A. Lyon, U. Gasser, and A. Fernandez-Nieves, J. Chem. Phys. **142**, 234905 (2015).
[18] G. Batchelor, J. Fluid Mech. **83**, 97 (1977).
[19] R. Borrega, M. Cloitre, I. Betremieux, B. Ernst, and L. Leibler, Europhys. Lett. **47**, 729 (1999).
[20] H. Senff and W. Richtering, J. Chem. Phys. **111**, 1705 (1999).
[21] U. Keiderling, Appl. Phys. A **74**, s1455 (2002).
[22] J. S. Pedersen, Adv. Colloid Interface Sci. **70**, 171 (1997).
[23] S.-H. Chen, Annu. Rev. Phys. Chem. **37**, 351 (1986).
[24] M. Kotlarchyk and C. Sow-Hsin, J. Chem. Phys. **79**, 2461 (1983).
[25] J. Hayter and J. Penfold, Mol. Phys. **42**, 109 (1981).
[26] D. Frenkel, R. Vos, C. De Kruif, and A. Vrij, J. Chem. Phys. **84**, 4625 (1986).
[27] N. Ashcroft and D. C. Langreth, Phys. Rev. **156**, 685 (1967).
[28] M. Ginoza and M. Yasutomi, J. Phys. Soc. Jpn. **68**, 2292 (1999).
[29] J. S. Pedersen, D. Posselt, and K. Mortensen, J. Appl. Crystallogr. **23**, 321 (1990).
[30] A. Fernandez-Barbero, A. Fernandez-Nieves, I. Grillo, and E. Lopez-Cabarcos, Phys. Rev. E **66**, 051803 (2002).
[31] K. Kratz, T. Hellweg, and W. Eimer, Polymer **42**, 6631 (2001).
[32] B. Zhou, U. Gasser, and A. Fernandez-Nieves, Nat. Commun. **14**, 3827 (2023).
[33] J. Wu, B. Zhou, and Z. Hu, Phys. Rev. Lett. **90**, 048304 (2003).
[34] U. Gasser, J.-J. Lietor-Santos, A. Scotti, O. Bunk, A. Menzel, and A. Fernandez-Nieves, Phys. Rev. E **88**, 052308 (2013).
[35] M. Urich and A. R. Denton, Soft Matter **12**, 9086 (2016).
[36] J. Brijitta and P. Schurtenberger, Curr. Opin. Colloid Interface Sci. **40**, 87 (2019).
[37] D. M. Heyes and A. C. Branka, Soft Matter **5**, 2681 (2009).